Journal of the Meteorological Society of Japan, Vol. 90A, pp. 259–274, 2012.
DOI:10.2151/jmsj.2012-A13

Nonlinearity of Land Carbon Sensitivities in Climate Change Simulations

Kaoru TACHIIRI

Japan Agency for Marine-Earth Science and Technology, Yokohama, Japan

Akihiko ITO

Japan Agency for Marine-Earth Science and Technology, Yokohama, Japan
National Institute for Environmental Studies, Tsukuba, Japan

Tomohiro HAJIMA, Julia C. HARGREAVES, James D. ANNAN and Michio KAWAMIYA

Japan Agency for Marine-Earth Science and Technology, Yokohama, Japan

(Manuscript received 10 March 2011, in final form 16 October 2011)

Abstract

In the climate-carbon cycle system, the terrestrial ecosystem feedback is significant. In studies on feedback analysis, the ecosystem feedback is divided into the sensitivity of carbon storage to atmospheric CO_2 concentration (β_L), and temperature change (γ_L). Although ecosystems include many nonlinear processes, the scenario- and time-dependency of β_L and γ_L have not been explicitly discussed. To check the validity of this simplification and its robustness, we carried out two, 1% per year (p.a.) increase and RCP4.5 scenario, experiments, using a process-based terrestrial ecosystem model forced by an existing GCM output, combined with an energy moisture balance model for the latter experiment, with 300 ensemble members perturbing twelve important and *a priori* unconstrained parameters. In the 1% p.a. experiment, β_L peaked around 500 ppm and then gradually decreased with increasing CO_2 level, while γ_L decreased with some inter-annual variability as temperature increases. The time-dependency of β_L was small (at least for CO_2 level > 550 ppm), but that of γ_L was significant, and the effect of this was larger than that of the nonlinear term (i.e., combined effect of CO_2 and temperature change). The scenario-dependency is also significant, but the effect in the estimated carbon uptake was smaller than that by the time-dependency. By investigating the background of this effect, we found that in the 1% p.a. CO_2 increase scenario, the maximum photosynthesis rate and specific leaf area (*SLA*, leaf area per unit dry mass) had the most significant contribution to both of β_L and γ_L, and the contributions are dependent on the climate state (i.e., temperature and atmospheric CO_2 level). For carbon uptake in both experiments, *SLA* and coefficient of plant respiration were most significant. We also attempted to constrain the ensemble members, and found that for net primary production, soil carbon and soil respiration, the default parameter set was already well-tuned, while observations of leaf area index (LAI) strongly constrains β_L, γ_L, airborne fraction and ecosystem carbon balance as the default model overestimated the LAI.

1. Introduction

The carbon cycle will have a significant impact on the future climate. The contribution of carbon cycle to the uncertainty in transient climate response is reported as about 40% of that of physical component (Huntingford et al. 2009). The positive feedback of carbon cycle to warming climate was first reported by Cox et al. (2000); by comparing

Corresponding author: Kaoru Tachiiri, Japan Agency for Marine-Earth Science and Technology, 3173-25 Showamachi, Kanazawa-ku, Yokohama, 236-0001, Japan.
E-mail: tachiiri@jamstec.go.jp

a full coupled and "uncoupled" (no climate-carbon cycle feedback) runs, the magnitude of the feedback was assessed as 250 ppm for IS92a (business as usual) scenario by HadCM3LC model. Friedlingstein et al. (2001) agreed with the sign of the feedback, but with significantly smaller magnitude (less than half) for the IPSL model. Friedlingstein et al. (2003) concluded that the reason for this difference is the difference in vegetation and soil carbon responses, in addition to the ocean CO_2 uptake controlled by the Southern Ocean circulation.

For the source of the terrestrial feedback, in Cox et al.'s (2000) study, soil carbon rather than vegetation carbon is the principal mechanism of positive climate-carbon cycle feedback. Jones et al. (2003) attempted to vary the temperature dependency of the soil respiration in the same model as Cox et al. (2000) and found that 25% of the uncertainty in climate-carbon cycle feedback was explained by this process. Dufresne et al. (2002) concluded that the discrepancy between Hadley and IPSL models are caused by difference of carbon allocation to vegetation and soil, and faster atmospheric warming in the Hadley model. Also, Matthews et al. (2005), by running an earth system model of intermediate complexity with four parameters for upper temperature constrain of photosynthesis, showed that varying photosynthesis parameter can significantly affect the soil carbon budget.

Given this background, Friedlingstein et al. (2006), summarizing the Coupled Climate-Carbon Cycle Model Intercomparison Project (C4MIP), concluded that all models simulated a positive climate-carbon cycle feedback, but there is large uncertainty among models, and the terrestrial ecosystem has larger values than marine ecosystem both in magnitude and uncertainty in the feedback. Friedlingstein et al. (2006) also proposed that the response of the climate-carbon cycle system to carbon emission can be described by three properties: linearised transient climate response (which they call α, in K ppm^{-1}), land and ocean carbon sensitivities to atmospheric CO_2 concentration (β, PgC ppm^{-1}), and land and ocean carbon sensitivities to temperature change (γ, PgC K^{-1}). Note that as well as being linearised, the use of a transient climate (temperature) response is somewhat scenario-specific and does not necessarily coincide with the IPCC definition of the temperature response after 70 years of a 1% per year (p.a.) rise in atmospheric CO_2. Similarly, as ecosystem models have many nonlinear processes, their responses to changing climate should be nonlinear, thus using single value for β and γ is contestable.

Matthews et al. (2007), by carrying out five runs varying some parameters related to photosynthesis and soil respiration, reported that the largest source of uncertainty in feedback strength of the terrestrial ecosystem to the climate change is photosynthesis-temperature response, and the difference in this property leads different γ, and then different magnitude of the total feedback.

Gregory et al. (2009) calculated the carbon cycle feedback, by doing full coupled, biogeochemically coupled (i.e., uncoupled) and radiatively coupled (CO_2 works as a greenhouse gas and induces climate change, but ecosystems feel a constant CO_2 concentration) runs for 1% p.a. concentration scenario. In that study, the airborne fraction, the ratio of the increase in airborne carbon to the accumulated carbon emission, is introduced as an important metric of total feedbacks. This is, combined with transient climate response, closely related to the discovery of a quasi-constant ratio of the temperature rise and the cumulative carbon emission (e.g., Allen et al. 2009; Matthews et al. 2009; Meinshausen et al. 2009).

In this study, by perturbing important parameters, we assess the validity of the linearisation in β and γ, and the range of uncertainty in sensitivity of the terrestrial ecosystem to changing CO_2 concentration and to climate change. We use the terrestrial ecosystem component (Sim-CYCLE, Ito and Oikawa 2002) of MIROC3.2-ESM, a state of the art earth system model (ESM) which participated in C4MIP with the name of "FRCGC". Unlike existing studies which have used at most only a handful of runs, we run 300 ensemble members to widely cover the possible parameter space. We achieve this by use of a "loosely coupled" (coupled only in the end of each year) earth system model emulator (JUMP-LCM, Tachiiri et al. 2010), in which a simplified physical model (MIROC-lite, Oka et al. 2010) is combined with a vegetation model, driven by output from a precalculated GCM run, thus emulating a full Atmosphere-Ocean-Vegetation General Circulation Model at much greater computational speed. To check the universality of the magnitude of the feedbacks, we applied two concentration scenarios, 1% p.a. incremental atmospheric CO_2 concentration increase and Representative Concentration Pathways (RCP, Moss et al. 2010) 4.5. The first experiment, inputting a steadily increasing CO_2 concentration to reach over

Table 1. Perturbed parameters and their ranges.

No.	Parameter	Label	Unit	Default	Perturbation range
p1	Maximum photosynthesis rate	PC_{sat0}	$\mu molCO_2\ m^{-2}s^{-1}$	8.0∼13.5*	−20∼+100% (of the default)
p2	Specific leaf area	SLA	cm^2 (g drymatter)$^{-1}$	110∼170*	−50∼+50% (of the default)
p3	Maximum light use efficiency	QE_0	$molCO_2$ (mol photon)$^{-1}$	0.05	0.047∼0.057 (C3, crop), 0.047∼0.071 (C4)
p4	Minimum temperature for photosynthesis	T_{MIN}	°C	−5.0∼11.0*	−3∼+3°C (of the default)
p5	Dependence of photosynthesis on intercellular CO_2 concentration	KM_{CD}	ppmv	10.0∼40.0*	−20∼+20% (of the default)
p6	Coefficient for specific maintenance respiration rate at 15°C	$SARM$	mgC (gC)$^{-1}$ day^{-1}	1.25∼1.62*	−30∼+70% (of the default)
p7	Coefficient of leaf life expectancy	SLF	Fraction day^{-1}	$1.23\sim3.20 \times 10^{-3}$*	−50∼+50% (of the default)
p8	Coefficient for allocation of assimilation	alloc_ass	(Dimensionless)	0.19∼0.30*	−50∼+50% (of the default)
p9	Coefficient for allocation of aboveground biomass	aloc_abg	(Dimensionless)	0.07∼0.52*	−50∼+50% (of the default)
p10	Coefficient for temperature dependency of plant's respiration	QT_0	(Dimensionless)	2.0	1.5∼3.0
p11	The 1st parameter for the temperature-dependency of soil decomposition	soil1	K	308.56	200∼340**
p12	The 2nd parameter for the temperature-dependency of soil decomposition	soil2	K	46.02	40∼60**

*: vegetation-type dependent; **: corresponding to Q10 of 1.5–3.0.

1200 ppm, is designed to investigate the model's basic characteristics, and the second experiment is for more practical purpose, i.e., to know what will likely happen in the near future.

The first objective of the study is to check the validity of the linearisation in β and γ. The second objective is to identify the important parameters that determine the magnitude of feedback of terrestrial ecosystem models (and natural terrestrial ecosystems). Once identified, future research may be focused on better evaluating these parameters, and thus projections of climate change may be better constrained.

2. Method

2.1 Models

a. Sim-CYCLE

In this study, the terrestrial vegetation model considered is Sim-CYCLE, a process based terrestrial carbon cycle model. As the detail of the model is described by Ito and Oikawa (2002), here we will put brief explanation focusing on our choice of perturbed parameters (listed as p1–p12 in Table 1).

The single-leaf photosynthetic rate (PC, mol CO_2 m^{-2} s^{-1}) is formulated as a Michaelis-type function of the incident Photosynthetic Photon Flux Density ($PPFD_{in}$, μ mol photons m^{-2} s^{-1}):

$$PC = PC_{sat} \cdot QE \cdot PPFD_{in} / (PC_{sat} + QE \cdot PPFD_{in}), \quad (1)$$

where PC_{sat} is PC for the light saturation condition; QE (mol CO_2 (mol photon)$^{-1}$) is light-use efficiency. PC_{sat} and QE are formulated as (maximum value) × (stress function), where the stresses are based on temperature, CO_2 level, air humidity and soil water (the parameters are different for C3, C4, crop plants) as follows:

$$PC_{sat} = PC_{sat0} \times F_{pc}(T) \times F_{pc}(CD_{ICL}) \times F_{pc}(SW) \quad (2)$$

and

$$QE = QE_0 \times F_{QE}(T) \times F_{QE}(CD_{ICL}). \quad (3)$$

Here PC_{sat0} and QE_0 are the potential maximum values for photosynthetic rate and light-use efficiency, which are perturbed in our experiments and listed as p1 and p3 in Table 1. $F_{pc}(T)$, $F_{QE}(T)$, $F_{pc}(CD_{ICL})$, $F_{QE}(CD_{ICL})$, $F_{pc}(SW)$ are functions which constrain photosynthetic activity using temperature, intercellular CO_2 concentration, and soil water condition. From PC, the instantaneous Gross Primary Production rate (GPP_{ins}, MgC ha^{-1}s^{-1}) is calculated under an assumption of exponential attenuation of photosynthetically active irradiance due to leaves' mutual shading.

$$GPP_{ins} = \int_0^{LAI} PC \cdot dLAI, \quad (4)$$

where LAI is Leaf Area Index calculated in Eq. (5):

$$LAI = 0.5SLA \cdot W_F, \quad (5)$$

where SLA, the Specific Leaf Area (ha MgC^{-1}), is perturbed parameter p2, and W_F (MgC ha^{-1}) is leaf biomass.

In Eq. (2), $F_{pc}(T)$ and $F_{pc}(CD_{ICL})$ are formulated as Eqs. (6) and (7):

$$F_{pc}(T) = \frac{(T - T_{MAX})(T - T_{MIN})}{(T - T_{MAX})(T - T_{MIN}) - (T - T_{OPT})^2} \quad (6)$$

and

$$F_{pc}(CD_{ICL}) = \frac{CD_{ICL} - CD_{CMP}}{KM_{CD} + CD_{ICL}}, \quad (7)$$

where in Eq. (6), T_{MAX}, T_{MIN}, and T_{OPT} (°C for all) are the maximum, minimum, and optimum temperatures for photosynthesis, respectively, and among these T_{MIN} is the fourth parameter perturbed (p4). On the other hand, in Eq. (7), KM_{CD} (ppmv) is a parameter of CO_2 sensitivity perturbed as p5, and CD_{ICL} and CD_{CMP} (ppmv for both) are the intercellular CO_2 concentration and CO_2 compensation point (at which the rate of photosynthesis equals the rate of respiration).

Autotrophic plant respiration consists of two components: the maintenance respiration, and the growth respiration. The amount of the maintenance respiration per unit existing carbon is an exponential function of temperature (°C) with a coefficient of so called $Q10$, while the growth respiration is proportional to a net biomass gain. Thus maintenance respiration (ARM, MgC ha^{-1}month^{-1}) is calculated as below:

$$ARM = SARM \cdot QT^{(T-15)/10} \cdot WP, \quad (8)$$

$$QT = QT_0 \cdot e^{\{-0.009*(T-15)\}}, \quad (9)$$

where T, QT and QT_0 are temperature, $Q10$ for ARM, and a coefficient to determine the temperature-dependency of plant respiration, of which the latter is p10. $SARM$ (MgC ha^{-1}s^{-1}), a function of the biomass, is the specific respiration rate perturbed by using a coefficient (p6). WP (MgC ha^{-1}) is the biomass of each of foliage, stem and root.

The seventh parameter p7 is a constant mortality or turnover rate (SLF, MgC MgC^{-1} day^{-1}) in the following equation for litterfall (LF, MgC ha^{-1} day^{-1}).

$$LF = SLF \cdot WP, \quad (10)$$

p8 and p9 are parameters related to the allocation of the produced carbon, which is distributed such that the fixed carbon is utilised by the plants most profitably to survive. Photosynthate is allocated first to foliage so that it becomes close to the optimal leaf area index maximizing daily net carbon uptake calculated from the daily GPP (Kuroiwa 1966). The rate of allocation to foliage is parameterised and perturbed as p8. After the carbon allocated to foliage is removed, a constant ratio (p9) of residual carbon is allocated to stem, and finally the remained part is distributed to root.

Soil organic carbon is divided into two components: the labile part of litter which circulates once in several months or a year, and the passive part in mineral soil which remains for decades or centuries. Thus, heterotrophic soil respiration (HR, MgC ha^{-1} day^{-1}) is composed of two components corresponding to these two. For both, temperature and soil moisture conditions are influential. For temperature dependency, an Arrhenius type function (Lloyd and Taylor 1994) of soil temperature (TS, °C) is used:

$$F_{HR}(TS) = e^{soil1\{1/soil2 - 1/(TS+46.02)\}}, \quad (11)$$

where values of soil1 and soil2 are 308.56 and 56.02 in the default model, and perturbed as p11 and p12 in the ensemble experiments. Equation (11) results in a temperature-dependent Q10, unlike TRIFFID

with a fixed Q10 value, used in Cox et al. (2000) and Jones et al. (2003).

In this study, the spatial resolution is T42 (128×64 grids to cover the globe), and effect of human land use is not considered.

b. JUMP-LCM

For the RCP4.5 scenario experiment, JUMP-LCM (Tachiiri et al. 2010), a system which couples a simplified atmosphere-ocean model (MIROC-lite, Oka et al. 2010) and a terrestrial ecosystem model (Sim-CYCLE, Ito and Oikawa 2002) by shell-scripting, is used. The system was designed to cover the limitation of MIROC-lite having a two dimension atmosphere in representing spatial distribution of some important variables for vegetation (e.g., precipitation and radiation). In this system the coupling process is organised as follows.

(1) MIROC-lite runs one year with a given CO_2 concentration (as a concentration scenario is used). As the marine carbon cycle is also included, the amount of CO_2 which is absorbed (or released) by the ocean is also calculated and stored for later analysis.
(2) The value of the global mean surface air temperature in MIROC-lite is used to pick a year from the preperformed MIROC3.2 GCM 1% per year increasing CO_2 run. In order to choose the year, a quadratic curve is used to smooth the annual mean temperature time series from the GCM data set. Thus the actual year chosen will have a mean temperature that differs from the smoothed value due to inter annual variability. For the appropriate year, daily climatic fields are extracted from the archive.
(3) The year's worth of daily climatic data from (2) and the CO_2 level of (1) are used to run Sim-CYCLE for one year, and we calculate the change in the total terrestrial ecosystem carbon storage. Then, return to (1).

In the current version of JUMP-LCM, the effect of the carbon budget is the only feedback from the ecosystems to the climate system. Other kinds of feedbacks, including effects of changed surface albedo and evaporation, are not considered. In JUMP-LCM, the MIROC-lite's resolution is $6^\circ \times 6^\circ$ (60×30 grids), with 15 ocean layers. The times step was 36 hours.

2.2 Ensemble experiments

Taking in account both the literature and the expert opinion of the Sim-CYCLE model developer (one of the co-authors of this study), we varied the parameters in Sim-CYCLE which have significant effects on the modelled terrestrial carbon cycle, and their ranges, as presented in Table 1. We used a Latin Hypercube to select 300 parameter sets uniformly across the whole parameter space.

Before the experiments, Sim-CYCLE was spun-up at 1850 with atmospheric CO_2 concentration of 285 ppm, using 25 years output of a MIROC3.2's control run for 2000 years (i.e., 80 repeats of the 25 years of forcing data), while MIROC-lite was spun-up at 1850 for 3000 years.

Using the equilibrated spin-up as the initial condition, we carried out the following two experiments, both of which are included in the Coupled Model Intercomparison Project Phase 5 (CMIP5) protocol. One is an ideal case considering only the CO_2 forcing increasing at a fixed rate for time designed to assess the model's basic behavior, and the other one is designed to assess the possible response of the earth system by giving a more realistic scenario. From the RCP scenarios, we chose RCP4.5 as this relatively eco-friendly but, perhaps, not unattainably extreme. This scenario is one of the two core RCP scenarios, and called a medium mitigation scenario in CMIP5 (Taylor et al. 2009)—another core scenario is RCP8.5, a high emissions scenario. By comparing the results from these scenarios, we can assess how the magnitude of feedback is different for different scenarios.

In the first experiment, for all ensemble members, daily output of the 1% incremental CO_2 increase concentration run of a GCM (an integration of the MIROC3.2 medium resolution version model) is input from 1st to 150th year (thus this is an off-line experiment). For this scenario we carried out three experiments: fully coupled, biogeochemically (BGC) coupled, and radiatively coupled cases. In a fully coupled run both of temperature and CO_2 concentration is increased. In the BGC coupled case, CO_2 concentration increases but that does not work as a green house gas (i.e., the air temperature does not increase). In the third case, on the other hand, temperature increases but the CO_2 concentration that the ecosystem senses is kept as 285 ppm. By comparing the results of these three experiments, we can calculate β and γ for land, and their variation in time.

For the second experiment we ran the model, JUMP-LCM, for the RCP4.5 concentration scenario (http://www.pik-potsdam.de/~mmalte/rcps/). The non-CO_2 forcing, including the effects of other

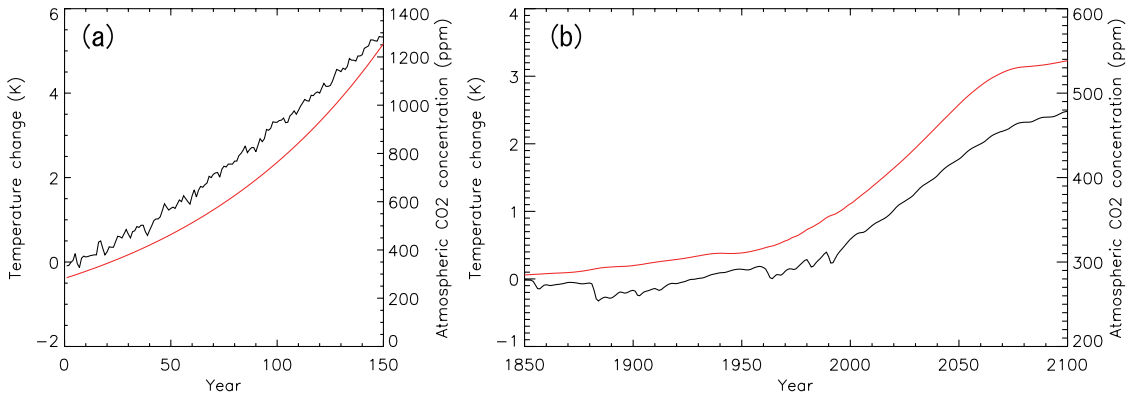

Fig. 1. Atmospheric CO_2 concentration and global mean surface air temperature for the two experiments. (a) The 1% p.a. scenario, (b) RCP4.5 scenario. For both of (a) and (b), black lines are temperature rise (using left axis) and red lines show the atmospheric CO_2 concentration (using right axis).

green house gasses, tropospheric/stratospheric aerosols and the variation of the solar activity, is considered as radiative forcing. By comparing the results from the two experiments we can assess the scenario-dependency of the feedback of the terrestrial ecosystem.

Atmospheric CO_2 concentration and change in the global mean surface air temperature for the two experiments are presented in Fig. 1.

2.3 *Metrics of feedbacks*

Among α, β, γ, the first one is a physical characteristic determined by the equilibrium climate sensitivity and ocean heat uptake efficiency, and other two are characteristics of biogeochemical cycles. There are two, terrestrial and marine, carbon-cycle components, so β and γ can be subdivided to those of land and ocean, and labeled β_L, β_O, γ_L and γ_O.

To get α, β, γ, Friedlingstein et al. (2006) compiled all participant models' outputs for two experiments using SRES A2 emission scenario: "coupled" (fully coupled) run and "uncoupled" (BGC coupled in this study) run. Then from these two runs they calculated α, β, γ with an assumption that β and γ work linearly (i.e., independently and additively). Rather than emission scenarios, Gregory et al. (2009) recommended concentration scenario experiments to simplify the feedback analyses. The accumulated total carbon uptake by ecosystem (C_u) can be written as follows:

$$C_u = C_\beta + C_\gamma = \beta C + \gamma T, \tag{12}$$

where C, T are change in airborne carbon and in temperature. C_β and C_γ are changes in ecosystem carbon storage due to changing CO_2 concentration, and temperature, respectively. For biogeochemically coupled (or "uncoupled") run the carbon uptake (C'_u) is as follows:

$$C'_u = \beta C. \tag{13}$$

And in Friedlingstein et al.'s (2006) approach, we have:

$$C''_u = C_u - C'_u = \gamma T, \tag{14}$$

where C''_u is carbon uptake in the radiatively coupled run. Equations (12)–(14) hold for the land subcomponent:

$$C_{uL} = \beta_L C + \gamma_L T, \tag{15}$$

$$C'_{uL} = \beta_L C, \tag{16}$$

$$C''_{uL} = \gamma_L T. \tag{17}$$

Gregory et al. (2009) showed that, although an approximately linear relationship was found for the temperature rise, the linear relationship ($C_u = C'_u + C''_u$) is not met for carbon uptake, and recommended to do three experiments including radiatively coupled run, so that β can be obtained from the biogeochemically coupled run, and γ can be from radiatively coupled run. Gregory et al. (2009) also showed the non-constancy of β, which depends on the rate of increase in CO_2 concentration.

An important metric to evaluate the combined effect of concentration-carbon (i.e., β) and the climate-carbon (γ) feedbacks is the cumulative airborne fraction, that is the ratio of increase in carbon in the atmosphere to the cumulative carbon emission, which for concentration scenario runs is

Table 2. Metrics of feedback.

Metrics	Unit	Reference	Note
(Concentration-carbon feedback)			
Carbon sensitivities to atmospheric CO_2 concentration (β)	PgC ppm^{-1} (or PgC PgC^{-1})	Friedlingstein et al. (2006)	β_L (β_O) for land (ocean)
(Climate-carbon feedback)			
Carbon sensitivities to temperature change (γ)	PgC K^{-1}	Friedlingstein et al. (2006)	γ_L (γ_O) for land (ocean)
(Overall feedback)			
Accumulated total carbon uptake by ecosystem (C_u)	PgC	Friedlingstein et al. (2006)	
Airborne Fraction (ratio of increase in airborne carbon to total carbon increase in air, ocean and land, A)	dimensionless	Gregory et al. (2009) etc.	
Carbon Climate Response	K PgC^{-1}	Matthews et al. (2009) etc.	Allen et al. (2009) defined Cumulative Warming Commitment (CWC) for the peak warming.

equal to the integrated allowable carbon emission (sum of carbon increases in atmosphere, land ecosystem, and marine ecosystem) (e.g., Gregory et al. 2009). By using this metric we attempt to combine β and γ to the change in the total carbon for RCP4.5 scenario, through the airborne fraction (A, Gregory et al. (2009)):

$$A = 1/(1 + \beta + \phi\gamma/\rho) = 1/(1 + \beta + \alpha\gamma), \qquad (18)$$

where $\phi = \frac{dF_c}{dC_A}$ (F_c and C_A are radiative forcing (W m^{-2}) and change in the atmospheric carbon content (PgC) relative to the pre-industrial state, ρ (W m^{-2}K^{-1})) is climate resistance, the sum of the climate feedback parameter and the ocean heat uptake efficiency. There is a relation between A, C_u and C_E (emitted carbon) as Eq. (19):

$$C_u = C_E - C_A = C_E \cdot (1 - A). \qquad (19)$$

Also, using A, the ratio of the temperature rise to the cumulative carbon emission is calculated. This ratio was named carbon climate response (CCR) by Matthews et al. (2009).

$$CCR = dT/dC_E = \left(\frac{dT}{dC_A}\right) \cdot \left(\frac{dC_A}{dC_E}\right) = \left(\frac{dF_c}{dC_A}\right) \cdot \left(\frac{dT}{dF_c}\right) \cdot A = \frac{\phi}{\rho} \cdot A. \qquad (20)$$

In this study, we first calculate the variation in time of β and γ, by evaluating them throughout a 1% p.a. experiment. Next, to assess the scenario-dependency of β and γ we attempted to estimate C_u for RCP4.5 using Eq. (12) by using β and γ calculated from 1% p.a. scenario. A and CCR are only used to check if our LCM could represent the basic characteristic of the existing ESMs.

The metrics mentioned in this sub-section are summarised in Table 2.

3. Results and discussion

3.1 Nonlinearity of β_L and γ_L

The resultant β_L and γ_L for the 150 year 1% p.a. experiment is presented in Table 3. Here, α is fixed as 0.0066 (K ppm^{-1}), the value of MIROC3.2 medium resolution version, which is slightly larger than the average of the C4MIP models. β_L and γ_L of our ensemble members are not so far from those of C4MIP models. β_L is smaller, both in the average and in dispersion, by about 20%, than those of C4MIP models, while γ_L is closer to C4MIP models. In the last row, γ_L(rad) which was directly calculated from the radiatively coupled run, is also presented to show the difference from γ_L(full-BGC), calculated from the difference of full-coupled and the biogeochemically (BGC) coupled experiments. The principal reason for difference be-

Table 3. Average and standard deviation of α, β_L, γ_L in 1% p.a. scenario experiment.

	Unit	This study	C4MIP
α	K ppm^{-1}	0.0066	0.0061 ± 0.0012
β_L	PgC ppm^{-1}	1.0 ± 0.5	1.3 ± 0.6
γ_L(full-BGC)	PgC K^{-1}	-79 ± 47	-79 ± 44
γ_L(rad)	PgC K^{-1}	-88 ± 42	—

Calculated up to 116th year (about 900 ppm). Values of C4MIP is for SRES A2 scenario (Friedlingstein et al. 2006). Presented are average $\pm$ standard deviation (of ensemble members for this study, and of models for C4MIP).

tween γ_L(full-BGC) and γ_L(rad) is the existence of the combined effect of temperature and CO_2 concentration in photosynthesis (Eqs. 2 and 3). Also, in Sim-CYCLE the optimum temperature for photosynthesis is dependent on CO_2 concentration. Another possible reason is that when temperature is increased, other climatic conditions including precipitation and humidity are changed and have an effect on the vegetation's activity. Moreover, soil respiration, proportional to soil carbon storage, is reduced in the radiatively coupled run and thus causes less carbon to be released.

Regarding the assessment of temperature rise using the cumulative emission, Fig. 2 presents the airborne fraction (A), the ratio of the temperature change to the airborne carbon (K PgC^{-1}), and CCR. Figure 2 shows non-equilibrium behavior in the 20th century, due to non-CO_2 (in particular aerosol) forcing, and equilibration after that. The nearly constant CCR is consistent with existing studies (e.g., Matthews et al. 2009), confirming that JUMP-LCM can represent some of the basic behavior of ESMs.

As indicated by the carbon uptake curve in Friedlingstein et al. (2006) and Gregory et al. (2009), there are some nonlinearities in β_L and γ_L, but β and γ are often presented as if they are model specific constants independent of scenarios and time. For careful analyses of ecosystem's feedback we must understand this nonlinearity, as the applicability of the linear approximation is the key to discussing general feedbacks by using β_L and γ_L determined by a certain level of CO_2 concentration in one scenario.

The change in β_L and γ_L for varying CO_2 concentration (for β_L) or temperature (for γ_L) for 1% p.a. scenario is presented in Fig. 3. Figure 3a and 3e present the relationship of land carbon to changing atmospheric CO_2 concentration for the biogeochemically coupled run (Fig. 3a) and to changing temperature for the radiatively coupled run (Fig. 3e).

Figures 3b and 3f show that, except for β_L in a low CO_2 concentration (< 400 ppm), both β_L and γ_L decrease with increasing CO_2 concentration or temperature. The processes causing this nonconstancy are as follows. For β_L, the shape of the function $F_{pc}(CD_{ICL})$ (Eq. 7) is saturating for high CO_2 concentration, and leaf area is also saturated for high NPP situation. For γ_L, the exponential functions of respiration on temperature (Eqs. 8 and 11) appear to be the principal reasons for the non-constancy.

Another result apparent from Fig. 3f is that the standard deviation of γ_L increases with temperature. One of the reasons for this may be the spatial variation in the magnitude of the warming. On the

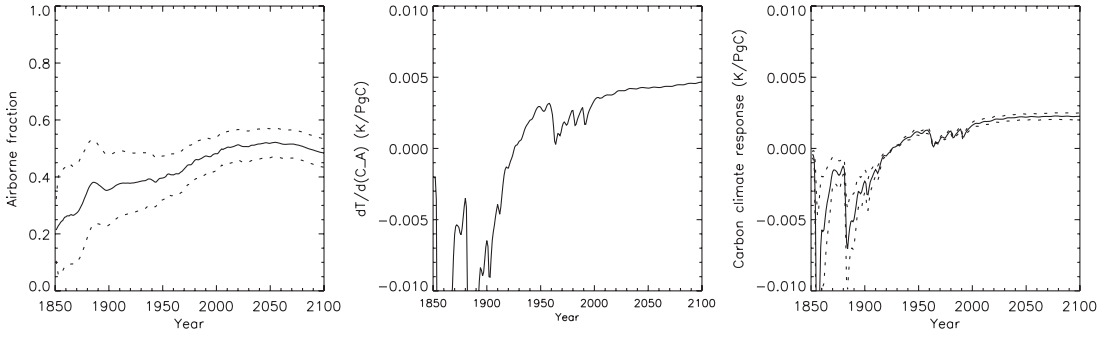

Fig. 2. Carbon Climate Response. (a): Airborne fraction (A) (b): dT/dC_A, the ratio of temperature change (K) to change in airborne carbon (PgC), (c): Carbon Climate Response. Average (solid) $\pm$ 1 standard deviation (dotted) are presented in (a) and (c).

other hand, the standard deviation of β_L does not show the same effect (Fig. 3b), and we note that, in our experiments, the CO_2 concentration is spatially uniform.

Figures 3c and 3g show the relationship between the values at the 66th and the 116th years for β_L (c) and γ_L (g). It is clear that β_L is more similar at the two time-slices than γ_L. On average β_{L116} is 13% smaller than β_{L66}, while γ_{L116} is, on average around 50% smaller (larger negative) than γ_{L66}, with a wider spread at large γ_L. The coefficients of determination for the linear regression in Figs. 3c and 3g are high for both β_L (0.95) and γ_L(0.98), but Fig. 3c shows some nonlinearity in β_L.

Figures 3d and 3h show the relationship between the values at the 116th and the 150th years for β_L (c) and γ_L (g). It is apparent that in comparison to below 900 ppm condition β_L is less constant for the higher CO_2 concentration condition, while γ_L is more constant. However, according to the coefficients of the regression line, β_L still has slightly more constancy than γ_L for the high CO_2 concentration condition. As in Fig. 3c, weak nonlinearity is apparent in Fig. 3d.

Another nonlinearity, the difference between γ_L calculated by the radiatively coupled run (γ_L(rad)), and that by the difference of full coupled and biogeochemically coupled runs (γ_L(full-BGC)), is shown in Fig. 4. Figures 4a and 4c show the relationship between the values obtained by two different methods, and Figs. 4b and 4d show the relative difference of these two values. For many ensemble members, the difference between the two values is around 20% of γ_L(rad), but the sign is opposite for the 66th and 116th years. For the 66th year, $\gamma_L(\text{rad}) > \gamma_L(\text{full-BGC})$, while for the 116th year $\gamma_L(\text{rad}) < \gamma_L(\text{full-BGC})$, indicating that the sign of the nonlinear term, determined by the combination of the above-mentioned reasons for the difference of γ_L(rad) and γ_L(full-BGC) can change for different CO_2 concentration and temperature.

From these results, it is concluded that a first order linearity may be assumed, although for more careful assessments it may be necessary to consider the effect of the nonlinearity.

In order to estimate the magnitude of scenario-dependency in β_L and γ_L, we assessed the land carbon uptake by using Eq. (15) to compare three kinds of nonlinearities in β_L and γ_L (Fig. 5): effect of combined term by CO_2 and temperature-dependency (black marks in Fig. 5a), time-dependency of β_L and γ_L (red marks in Fig. 5a),

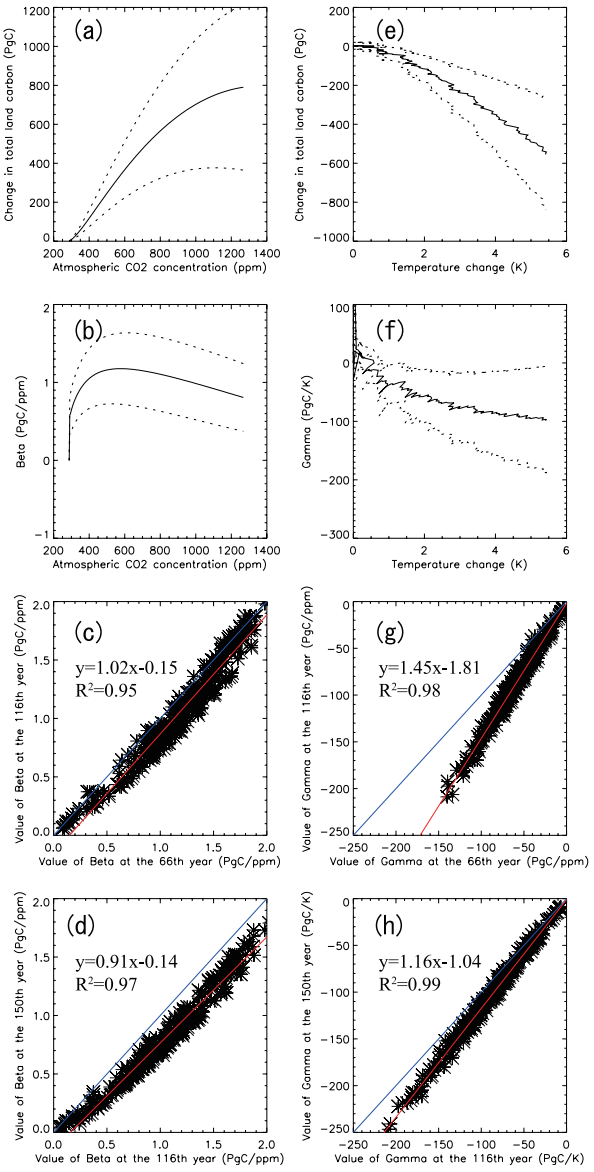

Fig. 3. Nonlinearity of land carbon sensitivities in the 1% p.a. experiment. (a) Change in land carbon for increasing CO_2 concentration in the BGC coupled run, (b) change in β_L, (c) Relationship between β_Ls calculated at the 66th and at the 116th years. (d) relationship between β_Ls calculated at the 116th and at the 150th years. The blue and red lines in (c) and (d) are $y = x$, and the regression line (the coefficients of the line and the coefficients of determination is also presented). (e) Change in land carbon for increasing air temperature in the radiatively coupled run, (f)–(h) are same as (b)–(d) but for γ_L.

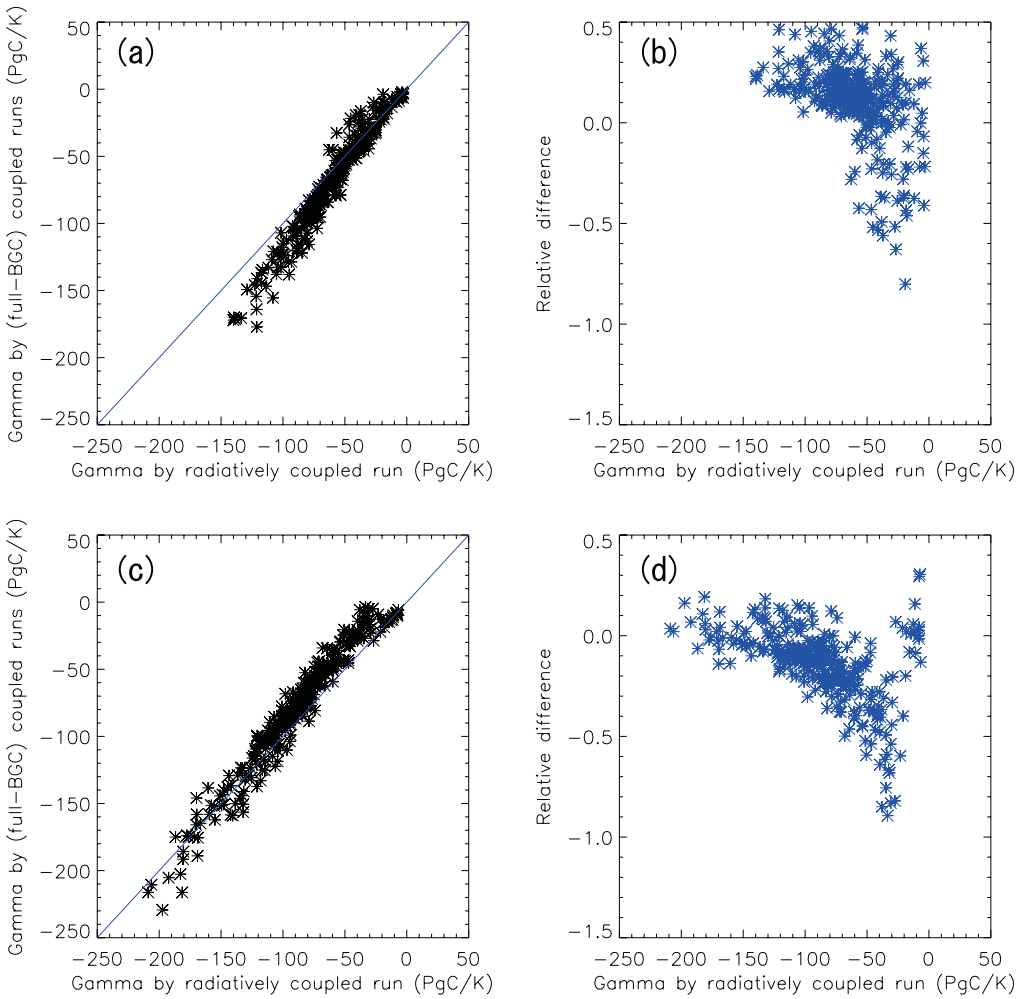

Fig. 4. Relationship between γ_Ls calculated by radiatively coupled run and by full-BGC coupled runs for 1% p.a. scenario. (a) The values calculated by full-BGC coupled run up to 66th year. The blue lines show $y = x$. (b) The difference of two methods (presented is $(\gamma_{full\text{-}BGC} - \gamma_{rad})/\gamma_{rad}$). (c) (d) are same as (a) (b) but for 116th year.

and scenario-dependency of β_L and γ_L (Fig. 5b). The RMSEs for the three plots are, 32, 76, and 55 PgC. As the first nonlinearity is included in the latter two plots, the RMSEs for time- and scenario-dependencies are calculated as 69 and 45 PgC by taking the square root of the MSE after subtracting the MSE of the first nonlinearity. From this result, for this case we can say that the scenario-dependency is larger than effect of nonlinear term, but smaller than the time-dependency, although the clear underestimation by β_L and γ_L calculated from the result of 1% p.a. CO_2 increase experiment presented in Fig. 5b is more striking than the dispersion of the red marks in Fig. 5a.

3.2 *What controls feedbacks?*

Table 4 depicts the coefficients of correlation between the perturbation in each of twelve parameters and β_L (or γ_L) for the 1% p.a. scenario. As presented in the Table, the maximum photosynthetic rate (PC_{sat0}) and specific leaf area (SLA) have the most significant effects on both of β_L and γ_L, and their effects have the same sign (i.e., positive and negative correlations to β_L and γ_L, respectively). In addition, the minimum temperature for photosynthesis (T_{MIN}) and the second parameter for the temperature-dependency of soil decomposition ($soil2$) have strong impacts with $<1\%$ level significance on both of β_L and γ_L. The coefficients of leaf

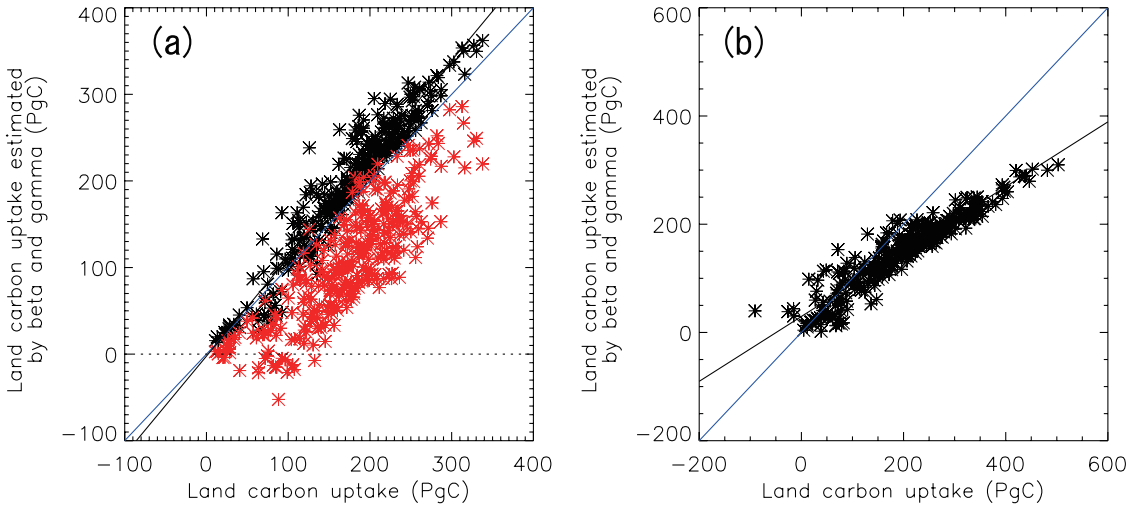

Fig. 5. Non-constancy in β_L and γ_L presented as the estimated C_{uL}. (a) Modelled and estimated C_{uL} by $\beta_L C + \gamma_L T$ up to 66th year for 1% p.a. scenario (C, T are change in atmospheric CO_2 concentration and in temperature from the first year). Black: estimation using β_L and γ_L up to 66th year, red: estimation using β_L and γ_L up to 116th year. Black and blue lines are regression line for black marks and $y = x$. (b) Modelled and estimated C_{uL} from 1850 to 2100 for RCP4.5 scenario. Estimation is using β_{L66} and γ_{L66} in 1% p.a. scenario. Black and blue lines are regression line and $y = x$.

Table 4. Coefficients of correlation between the perturbed parameters and β_L, γ_L, C_{uL} in 1% p.a. scenario (up to 116th year).

	β_L	γ_L
p1(PC_{sat0})	0.620***	−0.460***
p2(SLA)	0.574***	−0.494***
p3(QE_0)	0.027	−0.047
p4(T_{MIN})	−0.227***	0.310***
p5(KM_{CD})	−0.070	−0.075
p6($SARM$)	−0.136**	0.062
p7(SLF)	−0.129**	0.288***
p8(alloc_ass)	0.009	0.051
p9(aloc_abg)	0.139**	−0.102*
p10(QT_0)	−0.102*	−0.282***
p11(soil1)	−0.014	−0.083
p12(soil2)	−0.235***	0.386***

*/**/***: Significant at 10%/5%/1% level.

Table 5. Coefficients of correlation between the perturbed parameters and C_{uL} for 1% p.a. and RCP4.5 scenarios.

	1% p.a.	RCP4.5
p1(PC_{sat0})	0.237***	0.102*
p2(SLA)	0.628***	0.529***
p3(QE_0)	0.030	−0.002
p4(T_{MIN})	−0.008	0.096*
p5(KM_{CD})	−0.119***	−0.106*
p6($SARM$)	−0.180***	−0.177***
p7(SLF)	−0.009	0.109*
p8(alloc_ass)	−0.052	0.079
p9(aloc_abg)	0.237***	0.237***
p10(QT_0)	−0.457***	−0.583***
p11(soil1)	−0.112*	−0.154***
p12(soil2)	−0.046	−0.041

Values are up to 66th year (1% p.a.) or 2100 (RCP4.5). */**/***: Significant at 10%/5%/1% level.

life expectancy (SLF) and coefficient for temperature dependency of plant respiration (QT_0) also have strong effects on γ_L, while there are some other parameters which affect β_L at the 5% significance level. The reason why PC_{sat0} and SLA have most impact on β_L and γ_L may be because they explicitly appear in Eq. (4), while other parameters' effects on GPP are through relatively moderate cost functions. The change in photosynthesis affects soil carbon storage, and then soil respiration which is in proportion to the amount of soil carbon. This process also affects β_L and γ_L.

Table 5 shows the coefficients of correlations between the values of the perturbed parameters and the changes in the total terrestrial ecosystem carbon storage (C_{uL}) for 1% p.a. (up to the 66th year)

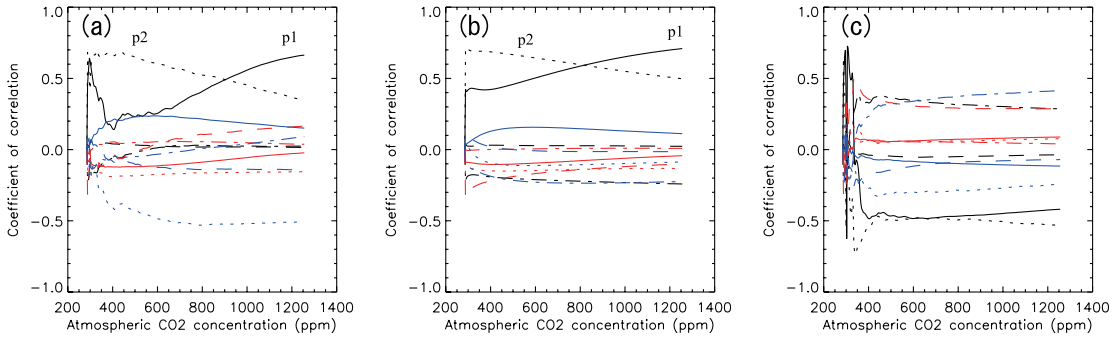

Fig. 6. Change in coefficient of correlation between parameter values and change in total land carbon in the 1% p.a. scenario. (a) To the total land carbon, (b) to β_L, (c) to γ_L. In all figures, black/red/blue lines are p1–4/p5–8/p9–12, solid/dotted/dashed/dash-dot lines are p1,5,9/p2,6,10/p3,7,11/p4,8,12.

and RCP4.5 (1850–2100) scenarios (i.e., around 550 ppm for both experiments). The results are mostly consistent between the two experiments, but some differences are found for PC_{sat0} (p1), SLA (p2) and QT_0 (p10). The contribution of β_L and γ_L to the total terrestrial carbon storage (through Eq. 15) is different for different scenarios, so this may explain the difference found.

It appears in Table 5 that SLA and QT_0 have the most contribution to C_{uL} for both scenarios. The strong correlation coefficients of QT_0 in Table 5 are a result of the same signs of coefficients between this parameter and β_L and γ_L, found in Table 4. Basically, the correlation presented to C_{uL} in Table 5 can be understood as combination of relationship of parameter values to β_L and to γ_L in Table 4, as formulated as Eq. (15). However, coefficients of correlation for some parameters in Table 5 are not explained by those in Table 4. Figure 6a presents the change in the coefficient of correlation between parameter values and C_{uL} in 1% p.a. increase scenario experiment. For most of all parameters correlations are reasonably equilibrated after 400 ppm, but PC_{sat0} (p1) and SLA (p2) are not equilibrated throughout the experiment. Figures 6b and 6c show this is principally due to the β_L's contribution. The CO_2 level of the Table 4 (for 1% p.a. scenario) and Table 5 (for two experiments) are 900 and 550 ppm, between which the contribution of PC_{sat0} and SLA can be significantly different.

To investigate the change in the contribution of PC_{sat0}, correlation at the 5th (about 300 ppm), 66th (about 550 ppm), 116th (about 900 ppm) and 150th (about 1270 ppm) year are presented in Fig. 7. In Figs. 7a and 7d (about 300 or 1270 ppm) a positive correlation between PC_{sat0} value and change in total carbon is observed. In Fig. 7b (550 ppm), there is a parabolic shape, leading to the low coefficient of correlation in Table 5. The relationship presented in Fig. 7c (900 ppm) is in between Figs. 7b and 7d.

In order to investigate the reason for the non-linear contribution of PC_{sat0} to C_{uL}, we carried out a small (of 11 members) ensemble only varying PC_{sat0} from 0.8 to 2.0 with a step of 0.12 for 1% p.a. concentration scenario. The relationships observed in Figs. 7b and 7c are observed for all of LAI, soil carbon, plant carbon, GPP, and NPP, as well as C_{uL}. By checking all related variables, we concluded that the parabolic curve apparent in Figs. 7b and 7c is originated from the CO_2 dependency of light use efficiency ($F_{QE}(CD_{ICL})$ in Eq. 3). This constrains the photosynthetic rate and reduces the optimum LAI, leading to a reduced GPP for high PC_{sat0} condition.

Similarly, we also carried out a small experiment only perturbing SLA, another parameter showing non-equilibrated behavior in Figs. 6a and 6b, but in that case the coefficient of correlation between SLA and C_{uL} is not decreased in later years of the 1% p.a. experiment. From this result it is indicated that the SLA's behaviour in Figs. 6a and 6b is an influence through other parameters' (principally the PC_{sat0}'s) effects.

3.3 *Constraint by observation data*

In the end of the analysis we consider the feasibility of constraining the parameters β_L, γ_L, the change in total land carbon storage, airborne fraction and the twelve perturbed parameters by using observation data for the carbon cycle, including LAI, net primary production (NPP), soil carbon

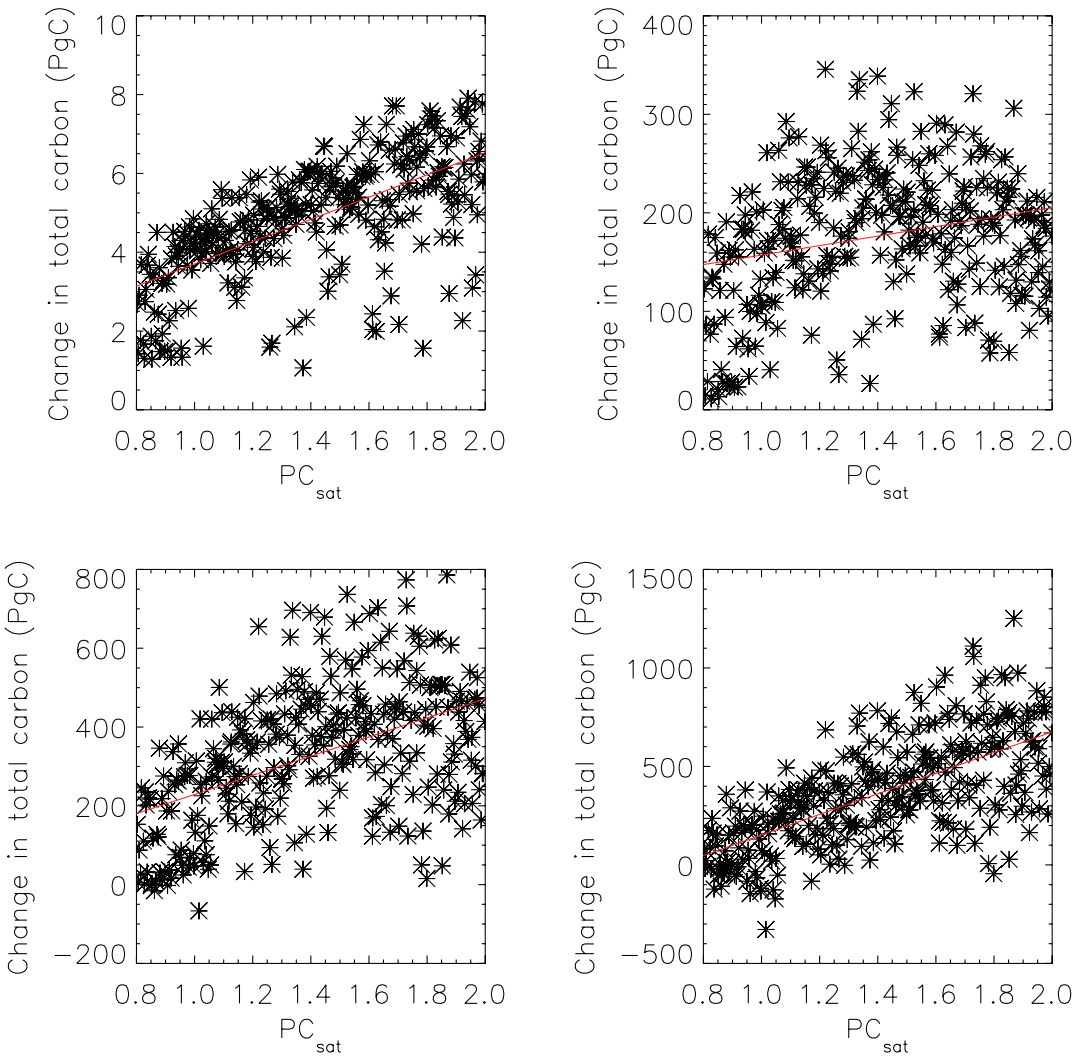

Fig. 7. Relationship between PC_{sat0} and the change in total carbon in the 1% p.a. experiment. (a) At the 5th year (about 300 ppm), (b) at the 66th year (about 550 ppm), (c) at the 116th year (about 900 ppm), (d) at the 150th year (about 1270 ppm). Red lines are linear regression.

storage, and soil respiration. The sources of the observation data are: 0.25×0.25 degree MODIS/LAI dataset (MCD15A2, https://lpdaac.usgs.gov/lpdaac/products/modis_products_table/leaf_area_index_fraction_of_photosynthetically_active_radiation/8_day_l4_global_1km/mcd15a), 0.5×0.5 degree grid cell NPP data by NPP multi-biome: Gridded estimates for selected regions worldwide, 1989–2001, R2 (Zheng et al. 2003), Global Soil Profile Data (ISRIC-WISE, Batjes 2000), and Global Annual Soil Respiration Data (Raich and Schlesinger 1992).

Except for the remotely sensed LAI data, the other three data sets are compiled from field-based data not covering the whole global land surface. We first resampled the data on to the model grid to use for validation (by taking the average if a grid contained multiple observation sites). For LAI data, average for each of four seasons (Dec–Feb, Mar–May, Jun–Aug, Sep–Nov) of 2003–2008 was calculated before being compared with model output, so that all data has only seasonal change and spatial variability (i.e., no inter-annual changes are considered here). They are resampled on to the T42

Table 6. Observational data used for constraint.

Data	Year of observation	No. of obs. points	No. of grids in T42[*1]	Model years compared	Reference
LAI	2003–2008[*2]	259200[**3]	1082	2003–2008	MCD15A2[*4]
NPP	1937–2001	2335	284	1961–1990	Zheng et al. (2003)
Soil carbon	1958–1993	319	60	1961–1990	Batjes (2000)
Soil respiration	1963–1992	171	48	1961–1990	Raich and Schlesinger (1992)

[*1]: Grids comparable with model, [*2]: monthly, [*3]: 0.25° grids, [*4]: https://lpdaac.usgs.gov/lpdaac/products/modis_products_table/leaf_area_index_fraction_of_photosynthetically_active_radiation/8_day_l4_global_1km/mcd15a.

grid before being compared to the model output. The information of these data is summarised in Table 6.

As weighting function, we used one designed along similar principles to the one used by Murphy et al. (2004). That is, we first calculated the ratio of the mean square error of each ensemble member to the spatial variance of the observed data, and using this ratio (called CPI' here, due to the similarity to Climate Prediction Index (CPI) in Murphy et al. 2004), the weight (W) is calculated as $W = \exp(-CPI'/2)$. For LAI, the weights are calculated for every season and then product of them was used as the weight for LAI. The weight is multiplied to β, γ, C_{uL} (1850–2100), A (1850–2100), and the twelve parameters of each ensemble member, to calculate the average and the standard deviation for comparing with the prior (i.e., unweighted).

Table 7 shows the result of the constraint of β, γ, C_{uL} (1850–2100), A (1850–2100), and the twelve parameters. The effect of LAI data gave relatively large impacts on some values. By LAI, the absolute values of β_L and γ_L are shifted smaller by around 45% and C_{uL} is shifted smaller by 35%. Among the parameters, not surprisingly SLA is most effectively constrained by LAI to smaller values than the default value by around 30%. Other variables have limited effects, except for some effect of the soil res-

Table 7. Prior and posterior distributions of β_L, γ_L (1% p.a. up to 900 ppm), change in total carbon (C_{uL}) and airborne fraction (A), and the twelve parameters for 1850–2100 in RCP4.5 scenario.

	Prior	Posterior (LAI)	Posterior (NPP)	Posterior (SoilC)	Posterior (SoilR)	Posterior (All)
β_L	1.046 ± 0.472	0.576 ± 0.302	1.018 ± 0.409	1.061 ± 0.457	1.122 ± 0.430	0.653 ± 0.268
γ_L	−88.1 ± 41.9	−49.0 ± 24.3	−87.1 ± 38.3	−89.2 ± 40.6	−93.5 ± 39.4	−50.9 ± 20.8
C_{uL}	200.1 ± 107.2	129.2 ± 81.67	201.9 ± 101.3	204.9 ± 106.5	217.5 ± 102.8	162.3 ± 80.5
A	0.484 ± 0.050	0.517 ± 0.042	0.483 ± 0.047	0.482 ± 0.050	0.476 ± 0.047	0.500 ± 0.040
PC_{sat0}	1.400 ± 0.347	1.351 ± 0.363	1.363 ± 0.336	1.396 ± 0.343	1.412 ± 0.335	1.394 ± 0.348
SLA	1.000 ± 0.289	0.690 ± 0.154	0.994 ± 0.275	1.012 ± 0.286	1.049 ± 0.278	0.703 ± 0.156
QE_0(C3, crop)	0.052 ± 0.003	0.052 ± 0.003	0.052 ± 0.003	0.052 ± 0.003	0.052 ± 0.003	0.052 ± 0.003
QE_0(C4)	0.059 ± 0.007	0.060 ± 0.007	0.058 ± 0.007	0.059 ± 0.007	0.059 ± 0.007	0.060 ± 0.007
T_{MIN}	0.000 ± 1.735	0.168 ± 1.806	−0.042 ± 1.742	−0.012 ± 1.727	−0.054 ± 1.715	0.032 ± 1.760
KM_{CD}	1.000 ± 0.116	1.020 ± 0.114	1.005 ± 0.116	0.998 ± 0.116	0.995 ± 0.116	1.004 ± 0.118
$SARM$	1.200 ± 0.289	1.367 ± 0.251	1.191 ± 0.286	1.195 ± 0.288	1.181 ± 0.284	1.374 ± 0.239
SLF	1.000 ± 0.289	0.990 ± 0.286	0.999 ± 0.291	1.000 ± 0.289	1.004 ± 0.289	0.999 ± 0.288
alloc_ass	1.000 ± 0.289	1.023 ± 0.291	0.995 ± 0.287	1.000 ± 0.288	1.002 ± 0.287	1.037 ± 0.285
aloc_abg	1.000 ± 0.289	0.977 ± 0.284	1.009 ± 0.287	0.997 ± 0.288	0.986 ± 0.287	0.879 ± 0.270
QT_0	2.250 ± 0.434	2.187 ± 0.437	2.246 ± 0.437	2.247 ± 0.433	2.258 ± 0.434	2.167 ± 0.447
soil1	270.0 ± 40.5	272.2 ± 40.8	269.9 ± 40.8	269.3 ± 40.3	270.1 ± 40.5	275.2 ± 41.8
soil2	56.06 ± 7.20	51.52 ± 6.04	60.36 ± 8.19	61.2 ± 9.15	62.44 ± 8.60	53.06 ± 5.36

Constrained by data of LAI, NPP, soil carbon (SoilC), and soil respiration (SoilR). Presented are average ± standard deviation.

piration data on γ_L, C_{uL} and a soil parameter (p12).

We also attempted a simple overall constraint by multiplying the weights of four variables, and the result is weakened effects of the above-mentioned constraints by individual variables. The LAI's effect on β_L, γ_L, C_{uL} and A also still remained in the overall constraint.

The result presented in Table 7 does not necessarily mean that LAI provides the best constraint on the model. That is, the almost unchanged posteriors for NPP, soil carbon and soil respiration suggest that the model was well-tuned for those variables. For LAI, however, significant overestimation was found for low to medium LAI value areas, and this overestimation is common for all seasons. The potential reasons for the overestimation are, effect of land use, effect of fire, and the subgridscale heterogeneity, all of which are not considered in this study.

4. Summary and conclusions

By carrying out a large (300 member) ensemble experiment, we assessed the validity of the linearisation in the sensitivity of land carbon storage to atmospheric CO_2 concentration (β_L), and to temperature change (γ_L).

The time-dependency of β_L was small (at least for CO_2 higher than 550 ppm), but that of γ_L was significant, and the effect of this was larger than that of the nonlinear term (i.e., combined effect of CO_2 and temperature change). It is indicated that the effect of scenario-dependency is also significant, although the error in the estimated carbon uptake was smaller than that by the time-dependency in β_L and γ_L.

In an idealised 1% p.a. CO_2 increase experiment, the maximum photosynthesis rate and specific leaf area, followed by the minimum temperature for photosynthesis, and a parameter on temperature dependency of the soil decomposition, are identified as significant parameters that influence the climate- and concentration-carbon cycle feedbacks. In this experiment we also found that the maximum photosynthesis rate and specific leaf area have unequilibrated contribution to β_L (and then C_{uL}) for the changing CO_2 concentration.

For C_{uL} up to 550 ppm, both for 1% p.a. and RCP4.5 scenarios, the specific leaf area and the temperature dependency of the plant respiration are the most significant parameters affecting the carbon budget.

From these results, in order to constrain the future temperature rise, we suggest to particularly reinforce observation on plant and soil respiration, maximum photosynthesis rate, specific leaf area, and the minimum temperature for photosynthesis. In addition, for maximum photosynthesis rate and specific leaf area, their dependency on temperature and CO_2 level should also be of interest.

Our attempt to constrain the model using observation data revealed that for NPP, soil carbon and soil respiration the model was well-tuned and the posterior probabilistic function is not significantly different from the prior distribution. But for LAI, significant overestimation by the model was found for wide low to medium LAI value regions.

The results obtained in this study are highly relevant to the problem of reducing the uncertainty in projecting the amount of CO_2 absorbed (or released) by the land ecosystem, and thus directly related to the socially critical question of how much carbon we can emit for a given CO_2 concentration pathway.

Acknowledgements

This work is supported by Innovative Program of Climate Change Projection for the 21st Century (of the Ministry of Education, Culture, Sports, Science and Technology, MEXT, Japan).

References

Allen, M. R., D. J. Frame, C. Huntingford, C. D. Jones, J. A. Lowe, M. Meinshausen, and Meinshausen, 2009: Warming caused by cumulative carbon emissions towards the trillionth tonne. *Nature*, **458**, 1163–1166.

Batjes, N. H. ed., 2000: *Global Soil Profile Data (ISRIC-WISE). [Global Soil Profile Data (International Soil Reference and Information Centre—World Inventory of Soil Emission Potentials)].* Data set. Available on-line [http://daac.ornl.gov/cgi-bin/dsviewer.pl?ds_id=547] from ORNL Distributed Active Archive Center, Oak Ridge National Laboratory, Oak Ridge, Tennessee, U.S.A. doi:10.3334/ORNLDAAC/547.

Cox, P. M., R. A. Betts, C. D. Jones, S. A. Spall, and I. J. Totterdell, 2000: Acceleration of global warming due to carbon-cycle feedbacks in a coupled climate model. *Nature*, **408**, 184–187.

Dufresne, J.-L., P. Friedlingstein, M. Berthelot, L. Bopp, P. Ciais, L. Fairhead, H. L. Treut, and P. Monfray, 2002: On the magnitude of positive feedback between future climate change and the carbon cycle. *Geophys. Res. Lett.*, **29**, 1405, doi:10.1029/2001GL013777.

Friedlingstein, P., L. Bopp, P. Ciais, J.-L. Dufresne, L. Fairhead, H. L. Treut, P. Monfray, and J. Orr, 2001: Positive feedback between future climate change and the carbon cycle. *Geophys. Res. Lett.*, **28**, 1543–1546.

Friedlingstein, P., P. Cox, R. Betts, L. Bopp, W. von Bloh, V. Brovkin, P. Cadule, S. Doney, M. Eby, I. Fung, G. Bala, J. John, C. Jones, F. Joos, T. Kato, M. Kawamiya, W. Knorr, K. Lindsay, H. D. Matthews, T. Raddatz, P. Rayner, C. Reick, E. Roeckner, K.-G. Schnitzler, R. Schnur, K. Strassmann, A. Weaver, C. Yoshikawa, and N. Zeng, 2006: Climate-carbon cycle feedback analysis, results from the C4MIP model intercomparison. *J. Climate*, **19**, 3337–3353.

Friedlingstein, P., J.-L. Dufresne, P. M. Cox, and P. Rayner, 2003: How positive is the feedback between future climate change and the carbon cycle? *Tellus*, **55B**, 692–700.

Gregory, J. M., C. D. Jones, P. Cadule, and P. Friedlingstein, 2009: Quantifying carbon cycle feedbacks. *J. Climate*, **22**, 5232–5250.

Huntingford, C., J. Lowe, B. Booth, C. Jones, G. Harris, L. Gohar, and P. Meir, 2009: Contributions of carbon cycle uncertainty to future climate projection spread. *Tellus*, **61B**, 355–360, doi:10.1111/j.1600-0889.2009.00414.x.

Ito, A., and T. Oikawa, 2002: A simulation model of the carbon cycle in land ecosystems (Sim-CYCLE): a description based on drymatter production theory and plot-scale validation. *Ecol. Model.*, **151**, 143–176.

Jones, C. D., P. Cox, and C. Huntingford, 2003: Uncertainty in climate carbon cycle projections assiciated with the sensitivity of soil respiration to temperature. *Tellus*, **55B**, 642–648.

Kuroiwa, S., 1966: *Dry matter production of plants, Ecology and Evolution, Iwanami Shoten, Tokyo, 71–100* (in Japanese).

Lloyd, J., and J. A. Taylor, 1994: On the temperature dependence of soil respiration. *Funct. Ecol.*, **8**, 315–323.

Matthews, H. D., M. Eby, T. Ewen, P. Friedlingstein, and B. Hawkins, 2007: What determines the magnitude of carbon cycle-climate feedbacks? *Global Biogeochem. Cy.*, **21**, GB2012, doi:10.1029/2006GB002733.

Matthews, H. D., M. Eby, A. J. Weaver, and B. J. Hawkins, 2005: Primary productivity control of simulated carbon cycle-climate feedbacks. *Geophys. Res. Lett.*, **32**, L14708, doi:10.1029/2005GL022941.

Matthews, H. D., N. Gillett, P. A. Stott, and K. Zickfeld, 2009: The proportionality of global warming to cumulative carbon emissions. *Nature*, **459**, 829–832.

Meinshausen, M., N. Meinshausen, W. Hare, S. C. B. Raper, R. Prieler, R. Knutti, D. J. Frame, and M. R. Allen, 2009: Greenhouse-gas emission targets for limiting global warming to 2°C. *Nature*, **458**, 1158–1163.

Moss, R., J. Edmonds, K. Hibbard, M. Manning, S. Rose, D. van Vuuren, T. Carter, S. Emori, M. Kainuma, T. Kram, G. Meehl, J. Mitchell, N. Nakicenovic, K. Riahi, S. Smith, R. Stouffer, A. Thomson, J. Weyant, and T. Wilbanks, 2010: The next generation of scenarios for climate change research and assessment. *Nature*, **463**, 747–756.

Murphy, J. M., D. M. H. Sexton, D. N. Barnett, G. S. Jones, M. J. Webb, M. Collins, and D. A. Stainforth, 2004: Quantifying uncertainties in climate change from a large ensemble of general circulation model predictions. *Nature*, **430**, 768–772.

Oka, A., E. Tajika, A. Abe-Ouchi, and L. Kubota, 2010: Role of the ocean in controlling atmospheric CO_2 concentration in the course of global glaciations. *Clim. Dynam.* doi:10.1007/s00382-010-0959-z.

Raich, J. W., and W. H. Schlesinger, 1992: The global carbon dioxide flux in soil respiration and its relationship to vegetation and climate. *Tellus*, **44B**, 81–99, Available on-line [http://daac.ornl.gov/cgi-bin/dsviewer.pl?ds_id=622].

Tachiiri, K., J. C. Hargreaves, J. D. Annan, A. Oka, A. Abe-Ouchi, and M. Kawamiya, 2010: Development of a system emulating the global carbon cycle in earth system models. *Geosci. Model Dev.*, **3**, 365–376.

Taylor, K. E., R. J. Stouffer, and G. A. Meehl, 2009: *A summary of the CMIP5 experimental design.* Available on-line [http://cmip-pcmdi.llnl.gov/cmip5/docs/Taylor_CMIP5_22Jan11_marked.pdf].

Zheng, D. L., S. D. Prince, and R. Wright, 2003: *NPP Multi-Biome: Gridded Estimates for Selected Regions Worldwide, 1989–2001, R1.* Available on-line [http://daac.ornl.gov/cgi-bin/dsviewer.pl?ds_id=614] from the Oak Ridge National Laboratory Distributed Active Archive Center, Oak Ridge, Tennessee, U.S.A. doi:10.3334/ORNLDAAC/614.